ERBE_S10n_Ed4.0

Data Quality Summary (July 12, 2017)

Investigation: **ERBE MEaSUREs**
Data Product: **ERBS-S10n**

Data set: **ERBS WFOV Nonscanner Instruments**

Data Set Version: **Edition4.0** **Release Date: July 12, 2017**

ERBE Ordering Tool: https://eosweb.larc.nasa.gov/project/measures/long-term-toa-m

This document provides a high-level quality summary of the Earth Radiation Budget Experiment (ERBE) data products containing flux at Top-of-Atmosphere (TOA) measured using Earth Radiation Budget Satellite (ERBS) Wide-Field-of-View (WFOV) nonscanner instruments. It only contains minimum information required to access the data quality. For more information, users are recommended to refer Wong et al. [2006], and https://eosweb.larc.nasa.gov/project/erbe/s10_table, including shrestha et. al., 2017 (in prepration).

Note:
There is a data gap in 1993 and 1998 due to instrument issues (see section 1.3). These years have months of missing data, thus users need caution while using data from these years.

TABLE OF CONTENTS

List of Tables

List of Figures

1 Introduction

The Earth Radiation Budget Experiment (ERBE) (https://science.larc.nasa.gov/erbe/, [Barkstrom, 1984]) was a National Aeronautics and Space Administration (NASA) space mission dedicated for measuring the Earth's top-of-atmosphere (TOA) broadband radiation fields using a constellation of three satellites (ERBS, NOAA-9, NOAA-10). The goal of this project was to better understand the Earth's climate by tracking the spatial patterns and temporal variability of the Earths radiation fields. Earth Radiation Budget Satellite (ERBS), a dedicated NASA science satellite, was launched on October 5, 1984 into a precessing orbit with a 57^o inclination and an altitude of 611 km. Its orbit precessed through the entire 24-hour local time every 72-day. The NOAA-9 and NOAA-10 satellites, both operational weather satellites maintained by National Oceanic and Atmospheric Administration (NOAA), were launched into Sun-synchronous orbits with 99^o inclinations and altitudes of 860 km orbit on December 12, 1984 and September 17, 1986, respectively. The equatorial crossing times for the NOAA-9 and NOAA-10 satellites were 1430 LT and 730 LT, respectively. While the NOAA-9 and -10 satellites provided global coverage, ERBS only viewed latitudes between 60^oN to 60^oS latitudes. Each of these satellites carried two ERBE instrument packages (Scanner and Nonscanner). While the Scanner instrument package scanned the Earth surface perpendicular to the satellite orbit track, the Nonscanner instrument package remained stationary and looked directly down on Earth at its nadir position. The ERBE scanner and nonscanner data product were processed independently using their own measurements. The ERBE data products included outgoing longwave (LW) radiation, reflected shortwave (SW) radiation, solar incoming radiation, and net downward radiation at TOA. The ERBE mission ended in October 14, 2005 with decommission of the ERBS satellite. This document provides a data quality summary of the latest reprocessed ERBE Wide-Field-of-View (WFOV) nonscanner Edition4 (Ed4) data product for the ERBS satellite (hereafter referred to as ERBS WFOV nonscanner Ed4) and includes a description of the data product, the changes in science algorithm, the results of data validation activities, the uncertainties in global annual mean, and cautions about using this data set.

1.1 Description of the ERBE Nonscanner Data Processing System

The ERBE nonscanner data processing system can be broken down into four major components. These components are 1) data telemetry, 2) merge, 3) inversion, and 4) time-space averaging. The telemetry process computes the telemetry data for a given day. The merge process computes the irradiance from the counts based on the available calibration coefficients. The inversion process converts the irradiance at satellite altitude to the TOA using the shape factor described by Green and Smith [1991]. Finally, the monthly time-space averaging (MTSA) process takes the instantaneous nonscanner footprint data and turns them into Level-3 spatially gridded and temporally averaged product.

1.2 History of the ERBS WFOV Nonscanner Data Product

The ERBS WFOV nonscanner data product is available to users from January 1985 to September 1999. This data product has gone through three major Edition changes (including the current Edition in this document) and one minor user-applied Revision. The natures of these data product changes are described below:

- **Original**: The original data is processed using the ERBE nonscanner WFOV scanner independent algorithm.
- **Edition2**: The original ERBS WFOV nonscanner data product contains large monthly mean time sampling errors; especially in higher latitude zones. This issue was corrected in the ERBS WFOV nonscanner Edition2 (Ed2) data product using a time sampling algorithm [Smith et al., 2015, Smith and Wong, 2016] by replacing monthly mean containing large sampling errors with a fill value.
- **Edition3**: The Ed2 did not include the effect of satellite altitude changes on the TOA fluxes. As the ERBS satellite altitude drop from 611 km to 585 km over the 15-year period, the uncorrected satellite altitude change caused an artificial increase in both TOA SW and LW fluxes over time. This artifact is corrected in ERBS WFOV nonscanner Edition3 (Ed3) data product by incorporating satellite altitude change in the data processing [Wong et al., 2006].

- **Edition3Rev1**: The Ed3 data contained a small residual artifact due to non-uniform degradation of the SW dome from exposures to direct sunlight. This artifact showed up as an increase with time in difference between daytime and nighttime TOA LW irradiances averaged over tropics (20^oN to 20^oS latitudes). The rate of increase is on the order of 2 to 3 Wm^{-2} per decade (Figure 3; Wong et al. [2006]). Because the change of the daytime and nighttime LW irradiance difference with time is not physical, the archived Ed3 data require a secondary user-applied Rev1 correction to both SW and LW irradiances so that the daytime and nighttime LW difference stays constant with time. Daytime LW irradiances are derived by subtracting SW irradiances (measured by the SW channel) from total (TOT) irradiances (measured by the TOT channel) during daytime. Because the SW channel has a filter, a degradation of the SW filter causes a drift of SW calibration. An uncorrected calibration drift leads to a trend in the daytime and nighttime LW irradiance difference.

- **Edition4**: This is the latest and current reprocessed data. Please see the rest of this document for changes in this Edition.

1.3 History of ERBS WFOV Nonscanner Instrument Anomaly

The ERBS WFOV nonscanner instrument had operated in space for a 20-year period from 1985 to 2005. During its first 15-year of nominal operations, the WFOV nonscanner instrument had experienced three minor anomalies which are caused by

1. Spacecraft battery power issue in the second half of 1993 (Lin et al. [2004], Smith and Bush [2005])

2. Spacecraft digital data recorder malfunction in March 1998

3. Spacecraft battery power issue for one month in December 1998

These three instrument anomalies had resulted in the loss of science data collection during their corresponding period. These science data gaps can be found in the ERBS nonscanner data record. **Science data user should pay attention to these data gaps in 1993 and 1998 when using the ERBS WFOV data product.**

In addition to these minor instrument issues, the nonscanner instrument package also suffered a major anomaly in October 1999. On October 5, 1999, the ERBS WFOV nonscanner instrument did not return to its nadir earth-view position [Smith and Bush, 2005] after the routine solar calibration operation and stopped at a position of approximately 16.2 degree off its normal nadir earth viewing position. Thus, all nonscanner footprint measurements after this point in time included a partial earth and space views. Due to the nature of this anomaly, the ERBS WFOV nonscanner science data product from October 1999 to August 2005 was not released to the publics pending further investigation. The ERBS WFOV nonscanner data product is therefore only available to users from January 1985 to September 1999.

2 Content of the ERBS WFOV Nonscanner Ed4 Data Product

The reprocessed ERBS WFOV nonscanner Ed4 data product contain level-3 time-space averaged irradiance estimates at the TOA for incoming solar, reflected solar, Earth-emitted, and net down-welling radiations. This Ed4 data product includes regional files at a 10^ox10^o resolution and time series of large-area means. The regional data is placed on the traditional ERBE grid system. The time series of large-area Mean (LAM) is derived for large areas over (1) 30^oN to 30^oS latitudes with 36-day means, (2) 60^oN to 60^oS latitudes with 72-day mean, and (3) the entire globe (90^oN to 90^oS latitudes) with 72-day and annual means. The content of the ERBS WFOV nonscanner Ed4 data product is listed in Table 1.

3 Improvements in the ERBS WFOV Nonscanner Edition4 Data

Using knowledge gained from both the Clouds and the Earth's Radiant Energy System (CERES) project [Priestley et al., 2000] and the ERBS WFOV nonscanner Ed3Rev1 data, the ERBS WFOV nonscanner Ed4 data incorporates number of changes to improve the characterization of the nonscanner instrument and their associated TOA radiation budget data with time. These changes are:

1. improving the unfiltering of ERBS WFOV nonscanner SW irradiances to be consistent

Table 1: Content of the ERBS WFOV nonscanner Ed4 Data Product

Temporal Resolution	**Spatial Resolution**	**Latitude range**
36-Day Regional Mean	10^ox10^o	30^oS to 30^oN
72-Day Regional Mean	10^ox10^o	60^oS to 60^oN
72DayAnnual Regional Mean	10^ox10^o	60^oS to 60^oN
36-Day LAM Time Series		30^oN to 30^oS
72-Day LAM Time Series		60^oN to 60^oS, 0^o to 60^oN, 0^o to 60^oS
Annual LAM Time Series		Global, 60^oN to 60^oS, 0^o to 60^oN, 0^o to 60^oS

LAM: Large-Area Mean

with that of the CERES unfiltering processing,

2. correcting for spectral dependence of the nonscanner SW dome degradation with time,
3. providing residual correction for day minus night LW irradiance difference trend
4. reworking the Ed3 satellite altitude change algorithm to be compatible with the other changes in the Ed4 processing
5. correcting satellite diurnal time sampling bias
6. incorporating time varying total solar irradiance data from the Solar Radiation and Climate Experiment (SORCE) project
7. tying the ERBE data to the absolute calibration of the CERES Energy Balanced and Filled (EBAF) data
8. estimating annual global mean fluxes

3.1 Unfiltering shortwave irradiances

The Ed4 data uses an algorithm similar to that used by the CERES for removing the effect of the instrument spectral filter response from SW radiance measurements [Loeb et al., 2001]. The irradiance with (filtered) and without (unfiltered) SW filter is computed at every 1^ox1^o resolution using International Satellite Cloud Climatology Project (ISCCP) [Schiffer and

Rossow, 1983] cloud fields. The unfiltering coefficient is then computed by taking the ratio of integrated filtered and unfiltered computed irradiances over the ERBS WFOV nonscanner instrument footprints.

3.2 Spectrally resolving shortwave filter degradation correction

The ERBE nonscanner SW channel contained a fused-silica dome in front of the activity cavity radiometer to filter out the LW irradiance. This SW dome had degraded spectrally and spatially over time due to exposure to direct solar radiation during spacecraft sunrise, sunset, and bi-weekly solar calibration event. To take into account of spectral dependent degradation of the filter function of ERBS SW WFOV (SWFOV) instrument, we assume in Ed4 that degradation of spectral dependent transmission changes with time following the expression:

$$T(\lambda) = [1 - exp(-\alpha\lambda)] * T_0(\lambda) \tag{1}$$

where, λ is the wavelength, α is the time dependent constant, and T_0 is the ERBS SWFOV original dome spectral response functions. The time dependent constant α is derived from data taken when the instrument viewed the sun. Because the solar spectrum is known, α can be derived from the broadband irradiance observations. The filter function at the beginning of the mission multiplied by the ratio of spectral dependent transmissions $T(\lambda)/T_0(\lambda)$ is the time dependent filter function that is used in the unfiltering process discussed above.

When Eq. (1) is used for the entire period of the ERBS instrument operation, it overestimates the degradation at shorter wavelength in later operational period. This leads to daytime-nighttime LW irradiance difference being over corrected over ocean where the reflected SW irradiance is dominated by shorter wavelengths. Therefore, we assume degradation of the filter function at shorter wavelength slows down or stops in July 1988 and use:

$$T_{fix}(\lambda) = [1 - 0.8 * exp(-\alpha_{fix}\lambda)] * T_0(\lambda).....\lambda <= 0.45\mu m \tag{2}$$

and

$$T(\lambda) = [1 - \beta * exp(-\alpha_{fix}\lambda^{0.1})] * T_0(\lambda).....\lambda > 0.45\mu m \tag{3}$$

where α_{fix} (=4.731028) is the value of α for July 1, 1988, and β is a time dependent constant derived based on the solar transmission.

3.3 Correction for Residual Day-minus-Night Longwave Difference Trend

The spectral dependence of SW filter degradation reduces the time dependent day-minus-night LW irradiances trend, however it does not completely eliminate it (Figure 1). Observing the time series of day-minus-night LW irradiances over 20^oN to 20^oS latitudes, we conclude that the drift is largely caused by several changes those occurred in three relatively short time periods: at around July 1986, around March 1987, and December 1993 (after the battery problem). Because these shifts occurred relatively in short time scales, they are hard to eliminate by considering the spectral degradation of the shortwave filter alone. In addition, this spectral unfiltering only accounts for the spectral nature of ERBS SWFOV dome degradation but does not account for the non-uniform spatial dome degradation [Smith et al., 2003].

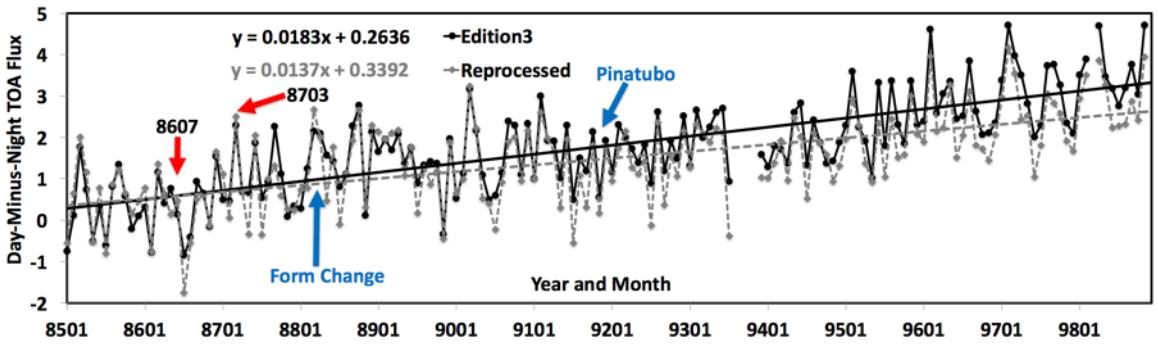

Figure 1: Time series of ERBS WFOV Nonscanner tropical mean ($(20^oN - 20^oS)$) at TOA monthly day-minus-night LW flux from 1985 to 1998 for Ed3 (black solid line with dot) and Ed4 (gray dashed line with dot). The linear regression slopes of these two time series are also plotted in the figure.

Following the correction described by Wong et al. [2006] a simple linear trend removal of the remaining slope is also applied to the Ed4 datasets. To remove this trend, a linear regression slope S is estimated such that tropical LW day-minus-night irradiance difference over 15-year period is zeroed out. This slope S varies among monthly, 36-day, and 72-day means and is used to compute the tropical adjustment factor as $S * (t - 1)$. This tropical

adjustment factor is then applied to Ed4 data, both for SW and LW. More information on this method is also available at https://asd-www.larc.nasa.gov/~tak/wong/Edition3_Rev1/.

3.4 Satellite Altitude Correction

Figure 1 in Wong et al. [2006] showed that the ERBS satellite altitude changed from 611 to 585 km over time. The effect on TOA irradiance estimate though small is significant. [Wong et al., 2006] show that the satellite altitude drop results in an artificial increase in both the SW and LW radiation by 0.6% over the 15-year period. The corrections to this altitude drop was already implemented in Ed3 dataset assuming near-circular orbit with inverse of the square distance relationship. Thus, this correction is not new to Ed4. However, the Ed3 altitude correction is implemented at the gridded level. For Ed4, the altitude correction is moved to the footprint level to be consistent with other changes in Ed4 algorithm.

3.5 Satellite Time Sampling Correction

ERBS was placed on a 57^o precessing orbit that required a full 72-day to sample the 24-hour diurnal cycle of radiation field on Earth. Because of this unique orbit, the ERBS nonscanner data contained significantly larger diurnal time sampling noise than other ERBE nonscanner data. While some of these noises had been reduced using the ERBE time-space averaging algorithm [Smith et al., 2015, Smith and Wong, 2016], it did not completely eliminate them in previous editions of the ERBS nonscanner data. To improve the ERBS nonscanner data, Ed4 data processing contains an additional regional correction to remove these residual time sampling bias. Satellite time sampling correction is derived by simulating ERBS samples with CERES observed flux. Over the course of one precession cycle (36 day between 30^oN to 30^oS latitudes and 72 days between 60^oN to 60^oS latitudes), ERBS samples a given location twice (once) a day for LW (SW) measurements. The sampling time within a day shifts over the course of one precession cycle. In addition, the overpass time at a given location for a given day of the year slowly drifts with year. To test the bias error in estimating a 36-day and 72-day means caused by this ERBS sampling, we make hourly TOA SW and LW climatology TOA irradiances from 14 years of CERES data in a 10^ox10^o resolution. We

then sample these irradiances according to the ERBS orbit. The difference of 36- or 72-day mean between CERES original irradiances and irradiances derived with ERBS sampling and CERES climatology is the bias error due to ERBS sampling. This also tests ERBS directional models and correction of sampling by ERBE MTSA algorithm. Figure 2 shows mean sampling errors in 72-day means in a 10^ox10^o resolution grids and Figure 3 shows the time series of annual mean irradiance over 60^oN to 60^oS latitudes from CERES (truth) and computed based on ERBS orbit sampling. Although the error at a 10^ox10^o scale is large (the RMS error is 49.7 (12.1) Wm^{-2} for SW (LW)), the error in a 30^oN to 30^oS or 60^oN to 60^oS latitudes is small (mean error is -0.9 (0.07) Wm^{-2} for SW (LW), -0.7 (0.07) Wm^{-2} for SW (LW)). The estimated sampling errors are then applied to both 36- and 72-day regional data products at a 10^ox10^o scale.

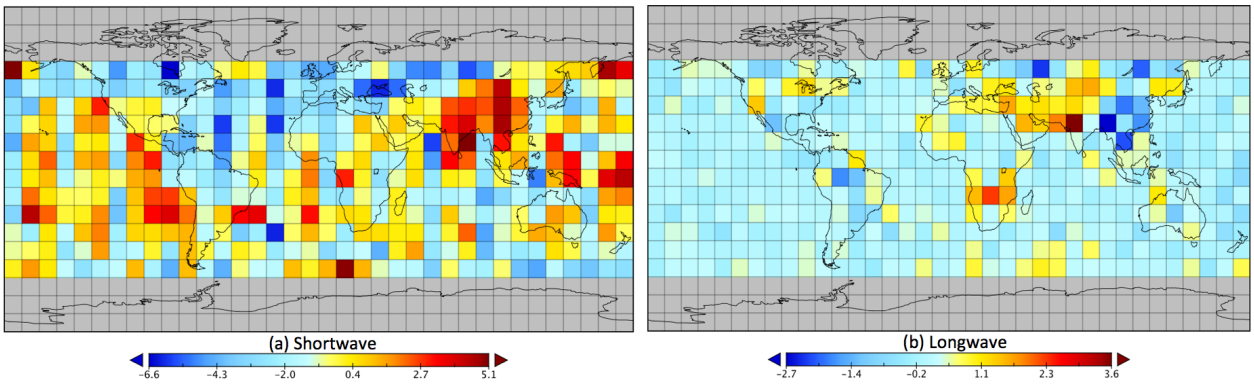

Figure 2: Estimated regional 10^ox10^o, 72-day mean satellite time sampling bias correction of TOA (a) Shortwave, and (b) Longwave fluxes for the 4th cycle of 72-day mean in 1985.

3.6 Incorporating Time Varying Total Solar Irradiance Data

The TOA daily solar incoming irradiance used in the ERBS Ed3 data processing is calculated assuming a constant Total Solar Irradiance (TSI) value of 1365 Wm^{-2} at 1-AU. This value does not change from year to year. Recent data produced by Kopp and Lean [2011], however, suggest a lower TSI value. Furthermore, the actual TSI at 1-AU changes significantly over time due to 11-year solar cycle. Thus, the incoming solar irradiance in the Ed4 data is updated with a time varying TSI dataset. The daily solar incoming irradiance for the ERBE

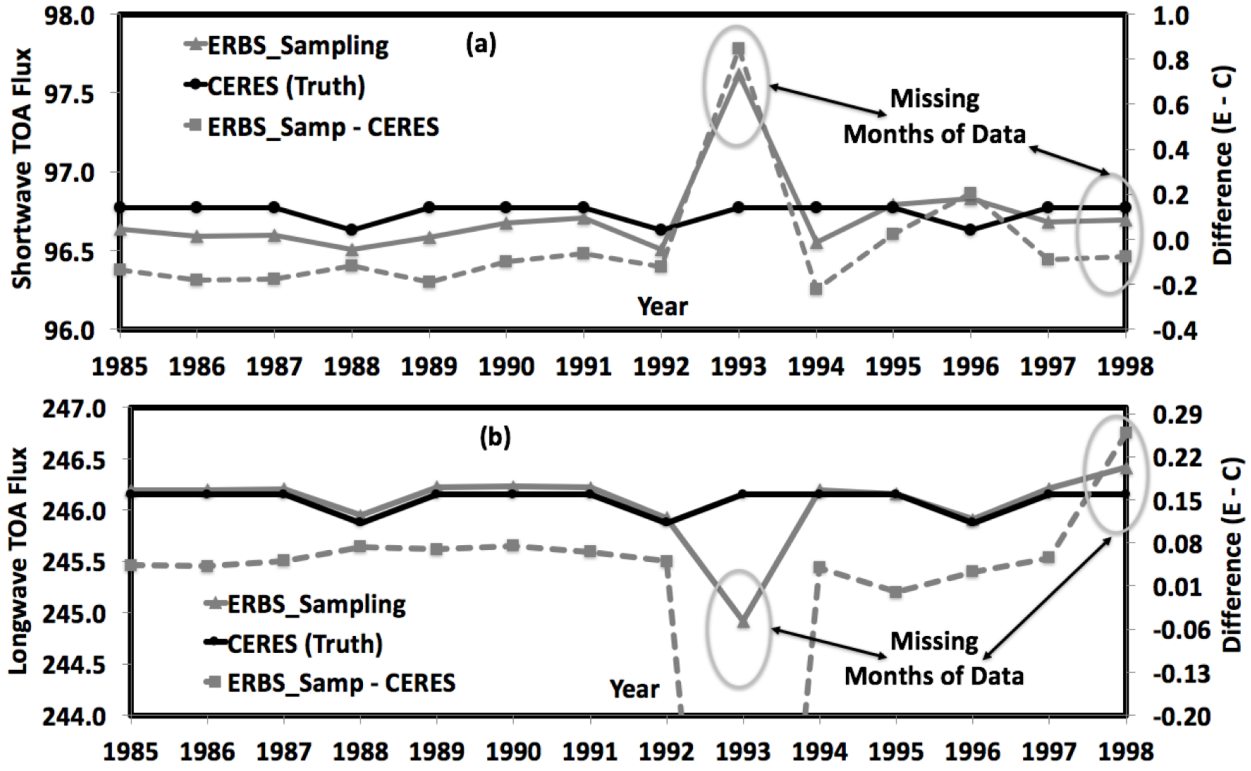

Figure 3: Estimated annual averaged, near-global ($60^o N$ to $60^o S$ latitudes) mean satellite temporal sampling bias of TOA (a) Shortwave, and (b) Longwave flux from 1985 to 1998

period comes from a composite dataset from the World Radiation Center (WRC) and is offset to match with those provided by SORCE. More information on this is available at https://ceres.larc.nasa.gov/science_information.php?page=TSIdata. Figure 4 shows the global annual mean solar incoming flux in the Ed3 product (Solid black line), while the updated Ed4 value is shown in grey dashed line. As Fig. 4 indicates, the Ed4 annual mean solar incoming flux is lower than those used in Ed3 product by close to 1 Wm^{-2}.

3.7 Tying ERBE Edition4 data to the absolute calibration of the CERES EBAF data

In order to have a consistent dataset that can be used for long term climate study, the ERBS WFOV Ed4 data is tied to the absolute calibration of the CERES EBAF Ed4 (https://ceres.larc.nasa.gov/products.php?product=EBAF-TOA) data product. The SW and LW

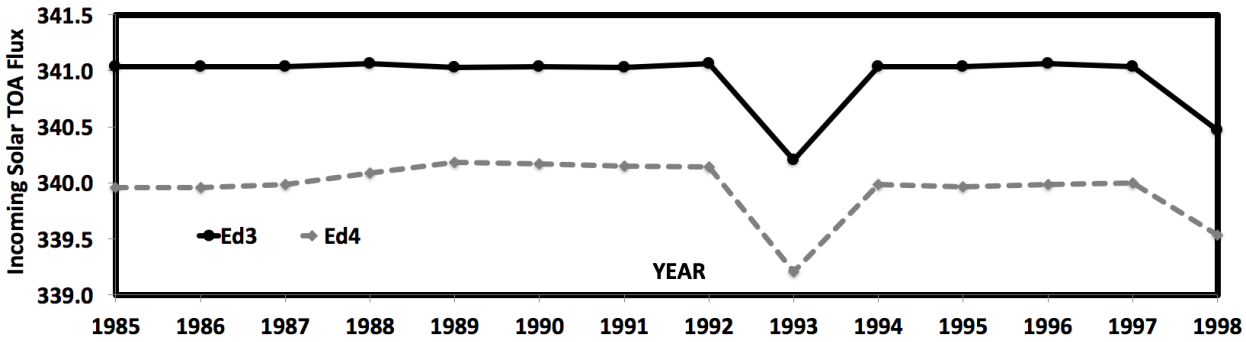

Figure 4: Annual mean time series of the TOA total incoming solar irradiance from 1985 to 1998 for Ed3 (solid black line) and Ed4 (gray dashed line) data

calibration transfer between these two datasets are performed independently in the following ways.

For the SW data, the ERBS WFOV Ed4 data is tied directly to the CERES EBAF data using a set of tilt-corrected ERBS WFOV data for the 3-year overlapped period from March 2000 to February 2003. The ERBS WFOV data during this period is processed using a special tilted instrument algorithm, developed to recover the ERBS WFOV nonscanner SW data record after the instrument anomaly on October 5 1999. These data recovery processes, involving the characterization of the tilted instrument and the retrieval of TOA SW flux, were discussed in details in Lee III et al. [2008] and Smith and Bush [2005], respectively. The difference in SW flux between ERBS WFOV Ed4 and CERES EBAF is computed by comparing the data from overlap period. Figure 5 shows the time series of 36-day mean SW irradiance over tropics (30^{o}N to 30^{o}S latitudes), where the black and grey solid line indicates, respectively CERES EBAF Ed4 irradiances and tilt-corrected ERBS irradiances during the tilted period. The average SW flux over all three years of data indicates that ERBS irradiance is lower than EBAF irradiance by 2.4 Wm^{-2}. Therefore, the entire Ed4 ERBS WFOV nonscanner SW data is raised by the value of 2.4 $Wm^{-2}2$ to match the absolute calibration of the CERES EBAF data.

For the LW flux, the ERBS nonscanner WFOV Ed4 data record is tied to the absolute calibration of the CERES EBAF data through the CERES-TRMM data. CERES-TRMM LW data overlapped with the ERBS nonscanner WFOV LW record from January to August

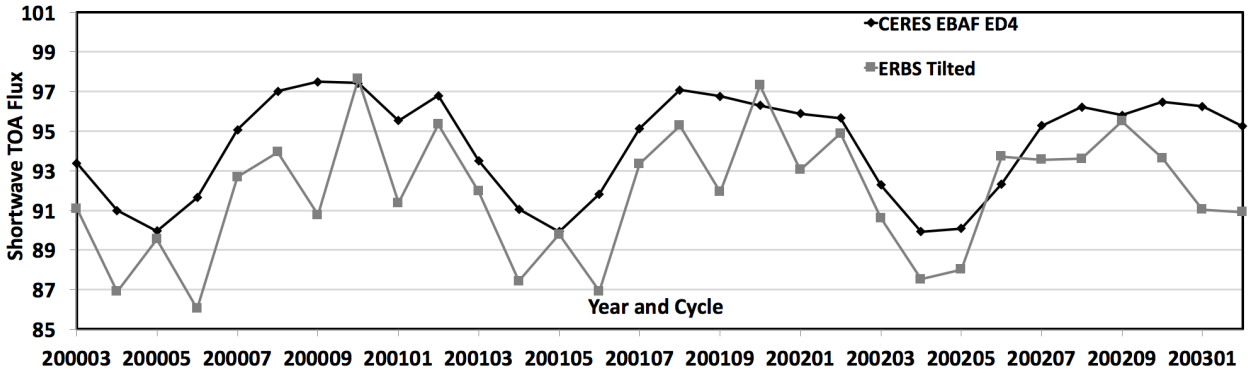

Figure 5: Time series of 36-day TOA mean SW flux over 30^oN to 30^oS latitudes from March 2000 to February 2003 for CERES EBAF Ed4 data (black line) and ERBS tilted WFOV nonscanner data (gray line)

1998. It also overlapped with the CERES EBAF LW data for March 2000. Using CERES-TRMM as an intermediate transfer point, CERES EBAF calibration is transferred to the ERBS nonscanner WFOV data in the following way. CERES-TRMM is first calibrated to the CERES EBAF absolute value using the one month overlapped data. The calibrated CERES-TRMM data is then used to transfer CERES absolute calibration to the ERBS WFOV Ed4 data using the 8-month overlapped data. Figure 6 shows the time series of TOA Monthly LW irradiances over the tropics. The ERBS nonscanner WFOV data before calibration are shown in the red solid line. The blue solid line is for CERES EBAF, black dot is for CERES-TRMM, and green solid line is ERBS nonscanner WFOV after calibration. The data in Figure 6 for March 2000 shows that the TRMM irradiance is lower than EBAF by 0.69 Wm^{-2} and the data in 1998 shows that the ERBS irradiance is lower than TRMM by 3.35 Wm^{-2}. Thus, the ERBS LW flux is 4.04 Wm^{-2} lower than the corresponding CERES EBAF data. Therefore, the entire Ed4 ERBS WFOV nonscanner LW data is raised by the value of 4.04 Wm^{-2} to match the absolute calibration of the CERES EBAF data.

3.8 Estimating global Annual mean irradiances

ERBS satellite did not sample the radiation field for the entire Earth. It only sampled the Earth between 60^oN to 60^oS latitudes. This section describes the procedures and corrections used in generating the global (90^oN to 90^oS latitudes) annual mean irradiance from ERBS

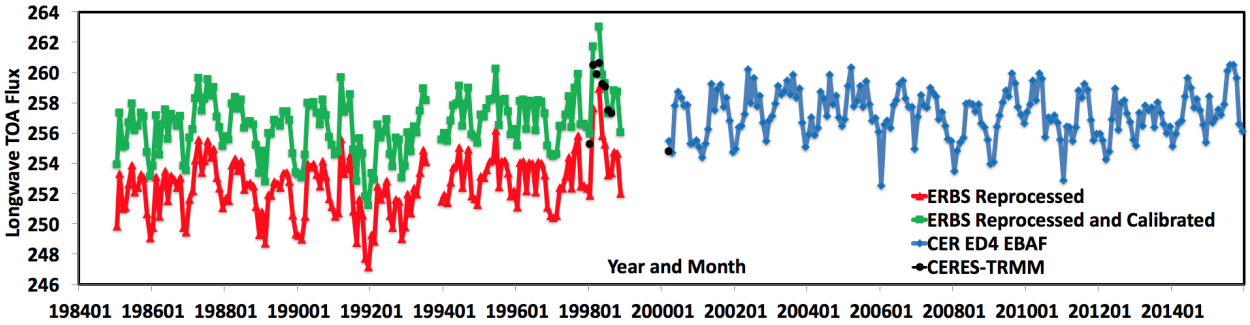

Figure 6: Time Series of Monthly LW Flux at TOA Over 30^{o}N to 30^{o}S

data. The global annual mean is calculated based on the 72-day regional mean data over 60^oN to 60^oS latitudes. First, the 72-day regional irradiances at a 10^ox10^o resolution are computed using daily mean data. There are five 72-day cycles (i.e., total of 360 days) in one calendar year. Ed4 also provides data for 36-day regional means over 30^oN to 30^oS latitudes and is computed in a similar way. There are ten 36-day cycles in one calendar year. Second, the 72-day annual mean regional data are then calculated based on the five 72-day regional mean values. Third, annual 60^oN to 60^oS large area mean is calculated by zonally averaging the 72-day regional data and area-weighted the zonal mean results. Fourth, the annual 60^oN to 60^oS large area mean is converted to annual global mean using a set of special conversion coefficients developed from CERES EBAF data. Finally, a last set of SW adjustment is made to correct for the effect of the missing 5 (non-leap year) or 6 days (leap year) in the annual mean calculation.

3.8.1 Computation of 72-day(36-day) regional means

Because of the precession of the ERBS orbit, daily mean values, especially the SW flux, depend heavily on the specific local measurement time. To mitigate this diurnal time sampling effects on the 72(36)-day mean SW irradiance, we first compute the albedo averaged over 72(36) days by Eq.(4) using only days when measurements were taken by dividing the sum of daily mean SW upward irradiance by the sum of the corresponding daily mean SW downward irradiance. We then multiply this by the 72(36)-day mean downward SW irradiance computed if the regions were sampled every day. The assumption is that the albedo, which

is the upward SW irradiance normalized by the downward SW irradiance, is less dependent on solar zenith angle than the SW irradiance. Therefore, the mean albedo with missing days within a 72(36)-day period is close to the mean albedo over a 72(36)-day period with no missing days. We apply this correction at a 10^ox10^o resolution grid.

$$\bar{\alpha} = 24 * \frac{\sum_{D_{SW}} M_{SW}(d)}{\sum_{D_{SW}} S(d)} \tag{4}$$

Here, $\bar{\alpha}$ is the average albedo from daily values, based on the sum of all integrated daily SW irradiance $M_{SW}(d)$. The $S(d)$ is the solar incidence, which is integrated from sunrise to sunset for each day with valid SW irradiance (D_{SW}). The day d varies from 1 to 72(36) for 72(36)-day mean, and only considers days when $M_{SW}(d)$ is valid. Thus, the 72(36)-day SW irradiance for a given region $\bar{M}_{SW}$ is then

$$\bar{M}_{SW} = \alpha * \sum_{d=1}^{N} \frac{S(d)}{24 * N} \tag{5}$$

Here, N is 72(36) for 72(36)-day mean.

3.8.2 Computation of 72DayAnnual regional means

The 72-day annual regional means over 60^oN to 60^oS is computed by taking average of five 72-day regional means from a given year. Thus, the 72-day annual regional means in the ERBS nonscanner WFOV Ed4 data is computed only using data from the first 360 days in a given year.

3.8.3 72-day global mean irradiance

Global mean irradiances are computed by scaling 72-day irradiance over 60^oN to 60^oS latitudes to 72-day global mean irradiance. In order to compute the 72-day scaling factor R_{72}, we compute the ratio of global mean and mean over 60^oN to 60^oS latitudes using Ed4 CERES EBAF TOA for complete months (i.e. January, February, April, June, July, September, and November). The scaling factor for months separated into two periods (i.e. March, may, August, October, and December) is computed with monthly mean from CERES EBAF TOA multiplied by the ratio of the irradiance averaged over the first or second half of the month

to the monthly mean irradiance from Ed3 SYN-1deg daily product. The scaling factor R is

$$R_{72} = \frac{F_{72,global}}{F_{72,60NS}} \tag{6}$$

Table 2 shows the five 72-day cycle scaling factors for converting the 60^oN to 60^oS latitudes mean to the global mean values along with scaling factors for northern and southern hemisphere. The standard deviations of the global mean scaling factor are 0.1240x10^{-2} and 0.0585x10^{-2} for SW and LW irradiance, respectively, indicating the robustness of their corresponding mean values.

Table 2: Mean and standard deviation of scaling factors derived with 14 years (from 2001 through 2014) of CERES data. Standard deviation is derived from averaging 5 standard deviations of the scaling factor for a 72-day period

	$F_{72,global}/F_{72,60^oNS}$		$F_{72,SH}/F_{72,0^o-60^oS}$		$F_{72,NH}/F_{72,0^o-60^oN}$	
	Shortwave	**Longwave**	**Shortwave**	**Longwave**	**Shortwave**	**Longwave**
Cycle-1	1.01857	0.96985	1.09973	0.97495	0.90134	0.96466
Cycle-2	0.99974	0.96856	0.92752	0.96168	1.05141	0.97547
Cycle-3	1.01652	0.97129	0.87562	0.95299	1.08709	0.98952
Cycle-4	0.98276	0.96800	0.97345	0.95429	0.99075	0.98175
Cycle-5	1.04841	0.97008	1.14759	0.97186	0.88485	0.96827
Mean	1.0132	0.9696	1.0048	0.9831	0.9632	0.9759
Standard deviation	$0.1240e^{-2}$	$0.0585e^{-2}$	$0.1157e^{-2}$	$0.1707e^{-2}$	$0.0836e^{-2}$	$0.0662e^{-2}$

As the 72-day annual regional mean is computed using only 360 days of data, the annual global mean computed from this regional data may differ from actual annual global mean computed from 365 days of data. The difference is small when data from both hemispheres are combined, it may, however, lead to significant differences when individual hemispheres are considered. Thus, to compute the actual annual global mean from 72-day annual regional means, an additional correction is implemented. The first correction takes account for an error due to 5 conversion factors R_{72} and the second correction takes account for hemispherical differences of incoming solar irradiance due to five 72-day means (or 360-day means) instead of 365-days means.

3.9 Effect of aerosol injected in the stratosphere by Mt. Pinatubo eruption on the reference level

Because of aerosols in stratosphere increased due to the Mt. Pinatubo eruption, the earth intercepts more direct solar radiation than it does before the eruption. To account for the larger effective earth radius, we need to increase the reference altitude discussed in Loeb and Kato [2002]. If we account for the reference altitude change due to aerosol injected in stratosphere, we need to increase the reference level from 20 km slightly. When the reference level increases slightly, SW irradiances are decreased accordingly. We, however, have not applied this correction to Ed4 ERBS TOA irradiance data and maintain the reference level of 20 km throughout the ERBS observation period.

4 Uncertainty in the annual global mean TOA irradiances derived from ERBS WFOV nonscanner

We assume that the uncertainty in the TOA global SW irradiance from ERBS WFOV nonscanner is due to instrument calibration, calibrating against CERES instruments, time and space sampling, and scaling to the irradiance between 60^oN to 60^oS latitudes to the global mean. The instrument calibration uncertainty is estimated in two ways. One is the uncertainty in the absolute calibration [Luther et al., 1986]. The other is the uncertainty in the stability, which is estimated from solar constant measurements [Lee III et al., 2004]. The uncertainty due to calibrating against CERES instruments is further divided into two components, the uncertainty of transferring the calibration from CERES to ERBS and uncertainty in CERES instrument calibration. All elements of the uncertainty are listed in Table 3. The total uncertainty is computed with the assumption that all components are independent, i.e. taking square root of the sum of square of all elements.

Table 3: Uncertainty (1σ) in the global annual mean TOA irradiances derived from ERBS WFOV nonscanner observations

Causes	**Shortwave(%)**	**Longwave(%)**	**Reference**
WFOV Calibration	2.5 (0.1)[1]	1.9 (0.1)[1],[2]	Luther et al. [1986], Lee III et al. [2004]
Calibration against CERES	0.3	0.1	
CERES Instrument Calibration	1.0	0.75	Loeb et al. [2009]
Inversion	Less than 1.0	0.5	
Time and Space Sampling	0.2	0.03	
Scaling 60^oN, 60^oS to global	0.1	0.1	
Total Uncertainty	2.9 (1.1)	2.0 (0.8)	

[1] Instrument stability uncertainty

[2] Both daytime LW, which is the same as SW, and nighttime LW uncertainties are 0.1%

5 Validation of the Edition4 data

The ERBE nonscanner Ed4 science team had performed the following validation activities to ensure the quality of this dataset and is reasonable and consistent with expectations. These activities include

1. SW stability check using Libya-4 desert
2. Comparisons with ERBS nonscanner WFOV Ed3Rev1 data
3. Comparisons with other radiation budget datasets

5.1 Stability of ERBS WFOV Shortwave Nonscanner Instrument

In order to evaluate the stability of the ERBS nonscanner WFOV Ed4 SW data, we generated a time series of SW flux over the Libya-4 desert site. This site is one of the stable targets used to assess stability of various satellite sensors [Teillet et al., 2007]. Figure 7 shows the time series of deseasonalized monthly mean SW irradiance over Libya-4. In order to isolate the effect of the Mt. Pinatubo in 1991 and instrument anomaly issues in 1993 and 1998 from this analysis, the deseasonalization is performed using data from 1985 to 1989. The quantitative result is listed in Table 4. For ERBS WFOV SW data, this table shows that the

average irradiance change in period 1994-1997 from 1985-1989 is only 0.1 Wm^{-2}, indicating a very stable instrument performance in the period from 1985 through 1998.

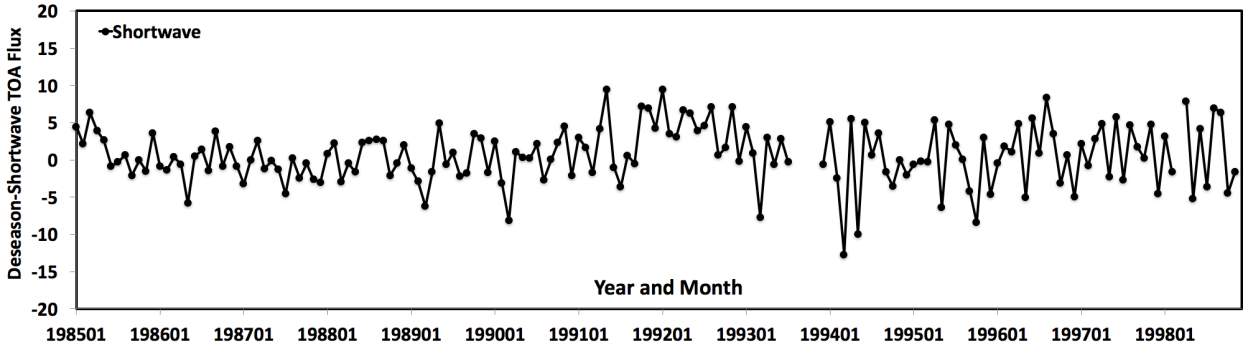

Figure 7: Time series of ERBS WFOV Ed4 deseasonalized monthly SW irradiance in Wm^{-2} over Libya-4 desert site. The deseasonalization is performed using data from 1985 to 1989 period

Table 4: Comparison of the ERBS WFOV Libya-4 SW flux statistics (mean ± one standard deviation in Wm^{-2}) between 1985-1989 and 1994-1997 period. These results are based on deseasonalized time series shown in Figure 7

Shortwave	**1985-1989 Period**	**1994-1997 Period**
Average	0.0 ± 2.6	0.1 ± 4.5

5.2 Comparison with previous ERBS nonscanner WFOV Edition3Rev1 data

In this section, we quantify the 60^oN to 60^oS large-area differences between this edition and earlier edition of the ERBS nonscanner data. Table 5 shows the comparison of Ed3Rev1 and Ed4 SW and LW data based on the average and standard deviation of monthly TOA irradiance anomalies over 60^oN to 60^oS latitudes. The Ed3Rev1 is the day-minus-night LWtrend correction applied to Ed3 datasets. To deseasonalize, the climatological mean of 1985-1989 is subtracted, and thus anomalies are defined with respect to this period. In addition, the entire dataset is divided into two periods: period-1 (1980's) from 1985-1989 and period-2 (1990's) from 1994 to 1997. The results shows that the decadal change over 60^oN to 60^oS latitudes in SW after reprocessing is the same as in Ed3Rev1, however the standard deviation has been greatly reduced to 3.2 Wm^{-2} from $8.0Wm^{-2}$. For LW, the

decadal change has been reduced to 0.6 Wm^{-2} from 1.0 Wm^{-2} in addition to reduction in standard deviation to 1.3 Wm^{-2} from 2.3 Wm^{-2}.

Table 5: Comparison of 60^oN to 60^oS large area mean of Ed3Rev1 and Ed4 Monthly TOA SW and LW flux anomaly (average ± one standard deviation in Wm^{-2}) for 1985-1989 and 1994-1997 period

	1985-1989 Period		**1994-1997 Period**	
	Ed3Rev1	**Ed4**	**Ed3Rev1**	**Ed4**
Shortwave	0.0 ± 1.1	0.0 ± 1.2	-2.7 ± 8.0	-2.8 ± 3.2
Longwave	0.0 ± 1.4	0.0 ± 0.7	1.0 ± 2.3	0.6 ± 1.3

5.3 Comparison with other radiation budget datasets

In this section, we compare the new Ed4 ERBS WFOV nonscanner data with other radiation budget datasets. Figure 8 shows the annual global mean time series for the ERBS WFOV nonscanner Ed4 TOA radiation in black dashed line, for CERES EBAF Ed4 in black solid line, and DEEP-C in blue solid line. DEEP-C data is described by Allan et al. [2014] and Liu et al. [2015] and is available from http://www.met.reading.ac.uk/~sgs02rpa/research/DEEP-C/GRL/. As mentioned earlier, to isolate the effect of Mt. Pinatubo in 1991 and instrument issue in 1993 and 1998 from our analysis to observe decadal change, the ERBE period is divided into two periods: period 1 (1980's) from 1985 to 1989 and period 2 (1990's) from 1994 to 1997. The results for reflected SW, outgoing LW, and net are shown in Table 6, 7, 8, respectively. These tables also contain results for CERES EBAF, ISCCP-FD [Zhang et al., 2004], and GEWEX-SRB (https://gewex-srb.larc.nasa.gov, Stackhouse et al. [2011], Zhang et al. [2013, 2015]) dataset. For SW, Table 6 shows that the ERBS and DEEP-C irradiance are consistent with each other in 1990's, while ERBS irradiance is higher than DEEP-C by 1.55 Wm^{-2} in 1980's. In addition, ERBS SW irradiance in 1990's is consistent with CERES irradiance in 2000's. In term of decadal change, the ERBS (DEEP-C, ISCPP-FD, GEWEX_SRB_Rel3) SW irradiance in 1990's is lower by -2.2 (-0.50, -1.46, -1.52) Wm^{-2} than in 1980's. Table 7 also shows that the ERBS LW irradiance is lower by -1.78(-0.72) Wm^{-2} compared to DEEP-C LW in 1980's(1990's). In term of decadal change, the ERBS

(DEEP-C, ISCPP-FD, GEWEX_SRB_Rel3) LW irradiance in 1990's is higher by 0.72 (-0.34, 0.17, 0.96) Wm^{-2} than in 1980's. Similarly, Table 8 for net imbalance shows that the net imbalance with ERBS (DEEP-C) is 0.45(0.17) Wm^{-2} in 1980's, while it is 1.89(0.96) Wm^{-2} in 1990's. As a comparison, the net imbalance for the CERES period in the 2000s is 0.62 Wm^{-2}. In term of decadal change, the ERBS (DEEP-C, ISCCP-FD, GEWEX_SRB_Rel3) net irradiance in 1990s is higher by 1.44 (0.79, 1.29, 0.56)Wm^{-2} than in 1980's.

Table 6: Average and Standard Deviations of a Time Series for Annual Reflected SW Radiation in Wm^{-2} from Figure 8a

Shortwave	**1985-1998**	**1994-1998**	**2001-2015**
ERBS	101.80 ± 0.48	99.59 ± 0.10	n/a
DEEP-C	100.25 ± 0.25	99.75 ± 0.27	n/a
CERES	n/a	n/a	99.23 ± 0.27
ISCCP-FD	105.69 ± 0.59	104.23 ± 1.07	n/a
GEWEX_SRB_Rel3	101.91 ± 0.28	100.39 ± 1.11	n/a

Table 7: Average and Standard Deviations of a Time Series for Annual Outgoing LW Radiation in Wm^{-2} from Figure 8b

Longwave	**1985-1998**	**1994-1998**	**2001-2015**
ERBS	237.79 ± 0.24	238.51 ± 0.18	n/a
DEEP-C	239.57 ± 0.30	239.23 ± 0.17	n/a
CERES	n/a	n/a	240.14 ± 0.25
ISCCP-FD	233.30 ± 0.69	233.48 ± 0.31	n/a
GEWEX_SRB_Rel3	237.58 ± 0.34	238.54 ± 0.64	n/a

6 Caution using the Data

As explained in section 1.3, there is a data gap in 1993 and 1998 due to instrument issues. These years have months of missing data, thus users need caution while using data from these years.

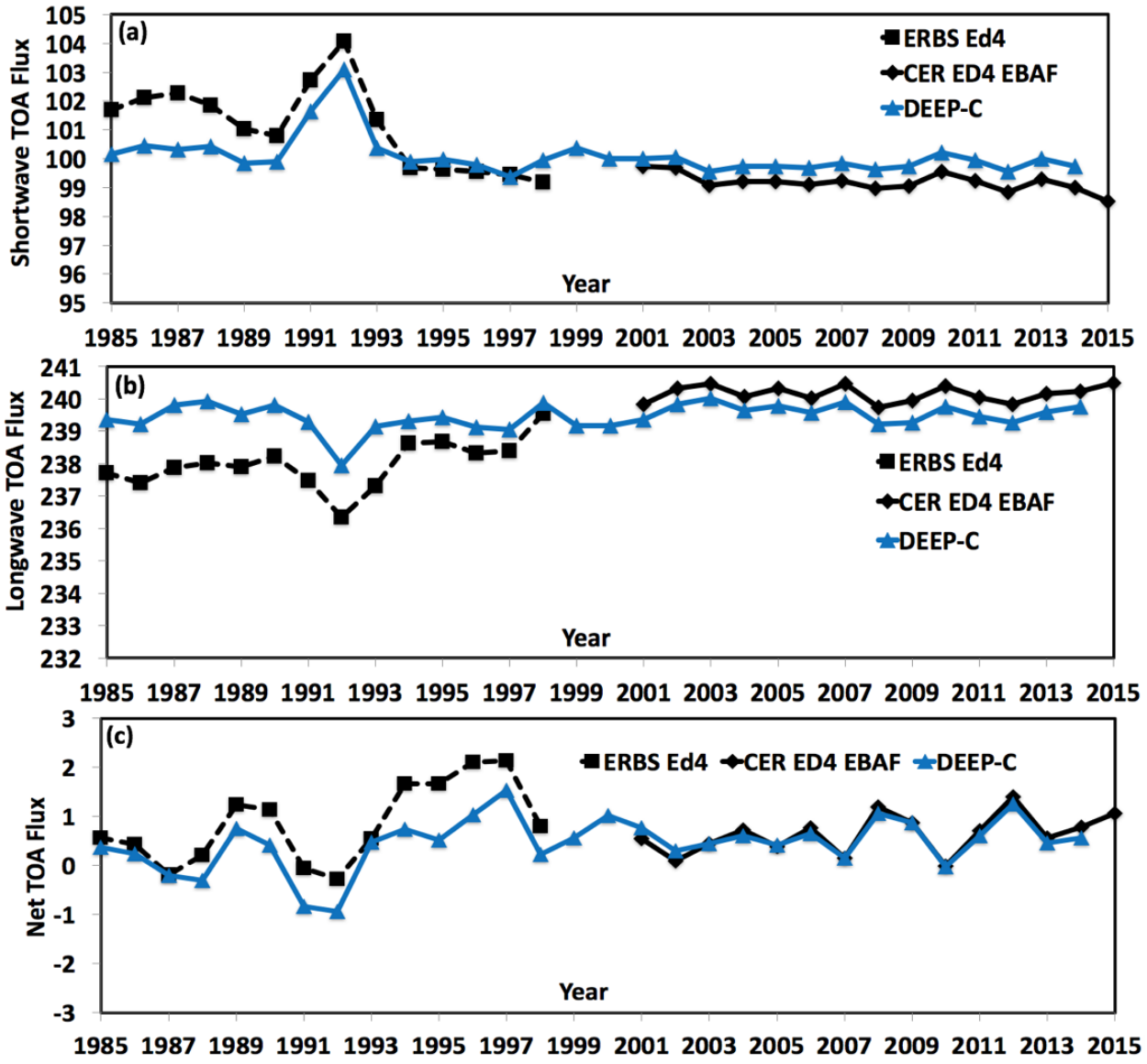

Figure 8: Time series of annual global (a) Shortwave, (b) Longwave, and (c) Net flux from 1985 to 2015

Table 8: Average and Standard Deviations of a Time Series for Annual Net Radiation in Wm^{-2} from Figure 8c

Net	1985-1998	1994-1998	2001-2015
ERBS	0.45 ± 0.52	1.89 ± 0.27	n/a
DEEP-C	0.17 ± 0.44	0.96 ± 0.44	n/a
CERES	n/a	n/a	0.62 ± 0.40
ISCCP-FD	2.79 ± 1.14	4.08 ± 0.87	n/a
GEWEX_SRB_Rel3	2.30 ± 0.51	2.86 ± 0.81	n/a

References

R. P. Allan, C. Liu, N. G. Loeb, M. D. Palmer, M. Roberts, D. Smith, and P.-L. Vidale. Changes in global net radiative imbalance 1985-2012. *Geophysical Research Letters*, 41 (15):5588–5597, 2014. ISSN 1944-8007. doi: 10.1002/2014GL060962. URL http://dx.doi.org/10.1002/2014GL060962.

B. R. Barkstrom. The earth radiation budget experiment (erbe). *Bulletin of the American Meteorological Society*, 65(11):1170–1185, 1984. doi: 10.1175/1520-0477(1984)065⟨1170:TERBE⟩2.0.CO;2. URL https://doi.org/10.1175/1520-0477(1984)065⟨1170:TERBE⟩2.0.CO;2.

R. N. Green and G. L. Smith. Shortwave shape factor inversion of earth radiation budget observations. *Journal of the Atmospheric Sciences*, 48(3):390–402, 1991. doi: 10.1175/1520-0469(1991)048⟨0390:SSFIOE⟩2.0.CO;2. URL https://doi.org/10.1175/1520-0469(1991)048⟨0390:SSFIOE⟩2.0.CO;2.

G. Kopp and J. L. Lean. A new, lower value of total solar irradiance: Evidence and climate significance. *Geophysical Research Letters*, 38(1):n/a–n/a, 2011. ISSN 1944-8007. doi: 10.1029/2010GL045777. URL http://dx.doi.org/10.1029/2010GL045777. L01706.

R. B. Lee III, R. S. Wilson, G. L. Smith, K. A. Bush, S. Thomas, D. K. Pandey, and J. Paden, editors. *On-orbit characterization of the Earth Radiation Budget Experiment*

broadband shortwave active cavity radiometers sensors response, volume 5660, 2004. doi: 10.1117/12.578822.

R. B. Lee III, G. L. Smith, T. Wong, and K. A. Bush, editors. *1999-2003 shortwave characterizations of Earth Radiation Budget Satellite (ERBS)/Earth Radiation Budget Experiment (ERBE) broadband active cavity radiometer sensors*, volume 7081, 2008. doi: 10.1117/12.797109. URL http://dx.doi.org/10.1117/12.797109.

B. Lin, T. Wong, B. A. Wielicki, and Y. Hu. Examination of the decadal tropical mean erbs nonscanner radiation data for the iris hypothesis. *Journal of Climate*, 17(6):1239–1246, 2004. doi: 10.1175/1520-0442(2004)017⟨1239:EOTDTM⟩2.0.CO;2. URL https://doi.org/10.1175/1520-0442(2004)017⟨1239:EOTDTM⟩2.0.CO;2.

C. Liu, R. P. Allan, P. Berrisford, M. Mayer, P. Hyder, N. Loeb, D. Smith, P.-L. Vidale, and J. M. Edwards. Combining satellite observations and reanalysis energy transports to estimate global net surface energy fluxes 19852012. *Journal of Geophysical Research: Atmospheres*, 120(18):9374–9389, 2015. ISSN 2169-8996. doi: 10.1002/2015JD023264. URL http://dx.doi.org/10.1002/2015JD023264. 2015JD023264.

N. G. Loeb and S. Kato. Top-of-atmosphere direct radiative effect of aerosols over the tropical oceans from the clouds and the earth's radiant energy system (ceres) satellite instrument. *Journal of Climate*, 15(12):1474–1484, 2002. doi: 10.1175/1520-0442(2002)015⟨1474:TOADRE⟩2.0.CO;2. URL https://doi.org/10.1175/1520-0442(2002)015⟨1474:TOADRE⟩2.0.CO;2.

N. G. Loeb, K. J. Priestley, D. P. Kratz, E. B. Geier, R. N. Green, B. A. Wielicki, P. O. Hinton, and S. K. Nolan. Determination of unfiltered radiances from the clouds and the earths radiant energy system instrument. *Journal of Applied Meteorology*, 40(4):822–835, 2001. doi: 10.1175/1520-0450(2001)040⟨0822:DOURFT⟩2.0.CO;2. URL https://doi.org/10.1175/1520-0450(2001)040⟨0822:DOURFT⟩2.0.CO;2.

N. G. Loeb, B. A. Wielicki, D. R. Doelling, G. L. Smith, D. F. Keyes, S. Kato, N. Manalo-Smith, and T. Wong. Toward optimal closure of the earth's top-of-atmosphere radiation

budget. *Journal of Climate*, 22(3):748–766, 2009. doi: 10.1175/2008JCLI2637.1. URL https://doi.org/10.1175/2008JCLI2637.1.

M. R. Luther, J. E. Cooper, and G. R. Taylor. The earth radiation budget experiment nonscanner instrument. *Reviews of Geophysics*, 24(2):391–399, 1986. ISSN 1944-9208. doi: 10.1029/RG024i002p00391. URL http://dx.doi.org/10.1029/RG024i002p00391.

K. J. Priestley, B. R. Barkstrom, R. B. L. III, R. N. Green, S. Thomas, R. S. Wilson, P. L. Spence, J. Paden, D. K. Pandey, and A. Al-Hajjah. Postlaunch radiometric validation of the clouds and the earths radiant energy system (ceres) proto-flight model on the tropical rainfall measuring mission (trmm) spacecraft through 1999. *Journal of Applied Meteorology*, 39(12):2249–2258, 2000. doi: 10.1175/1520-0450(2001)040⟨2249:PRVOTC⟩2.0.CO;2. URL https://doi.org/10.1175/1520-0450(2001)040⟨2249:PRVOTC⟩2.0.CO;2.

R. A. Schiffer and W. Rossow. The international satellite cloud climatology project (isccp): The first project of the world climate research programme. *Bull. Amer. Meteor. Soc.*, 64: 779–784, 1983.

G. L. Smith and K. A. Bush, editors. *Retrieval of radiation fluxes from tilted wide field-of-view radiometer measurements*, volume 5979, 2005. doi: 10.1117/12.626567. URL http://dx.doi.org/10.1117/12.626567.

G. L. Smith and T. Wong. Time-sampling errors of earth radiation from satellites: Theory for monthly mean albedo. *IEEE Transactions on Geoscience and Remote Sensing*, 54(6): 3107–3115, June 2016. ISSN 0196-2892. doi: 10.1109/TGRS.2015.2503982.

G. L. Smith, R. B. Lee III, and J. Paden, editors. *Dome Degradation Pattern of ERBE Wide Field-of-View Shortwave Radiometer*, volume 4881, 2003. doi: 10.1117/12.462516. URL http://spie.org/Publications/Proceedings/Paper/10.1117/12.462516.

G. L. Smith, T. Wong, and K. A. Bush. Time-sampling errors of earth radiation from satellites: Theory for outgoing longwave radiation. *IEEE Transactions on Geoscience and Remote Sensing*, 53(3):1656–1665, March 2015. ISSN 0196-2892. doi: 10.1109/TGRS.2014.2338793.

P. W. Stackhouse, S. K. Gupta, S. J. Cox, T. Zhang, J. C. Mikovitz, and L. M. Hinkelman. The nasa/gewex surface radiation budget release 3.0 24.5-year dataset. *GEWEX News*, 21 (1):10–2, 2011.

P. M. Teillet, J. A. Barsi, G. Chander, and K. J. Thome, editors. *Prime candidate Earth targets for the post-launch radiometric calibration of space-based optical imaging instruments*, volume 6677, 2007. doi: 10.1117/12.733156. URL http://dx.doi.org/10.1117/12.733156.

T. Wong, B. A. Wielicki, R. B. L. III, G. L. Smith, K. A. Bush, and J. K. Willis. Reexamination of the observed decadal variability of the earth radiation budget using altitude-corrected erbe/erbs nonscanner wfov data. *Journal of Climate*, 19(16):4028–4040, 2006. doi: 10.1175/JCLI3838.1. URL https://doi.org/10.1175/JCLI3838.1.

T. Zhang, P. W. Stackhouse, S. K. Gupta, S. J. Cox, J. C. Mikovitz, and L. M. Hinkelman. The validation of the gewex srb surface shortwave flux data products using bsrn measurements: A systematic quality control, production and application approach. *Journal of Quantitative Spectroscopy and Radiative Transfer*, 122:127 – 140, 2013. ISSN 0022-4073. doi: http://dx.doi.org/10.1016/j.jqsrt.2012.10.004. URL http://www.sciencedirect.com/science/article/pii/S0022407312004335. INTERNATIONAL SYMPOSIUM ON ATMOSPHERIC LIGHT SCATTERING AND REMOTE SENSING (ISALSaRS11).

T. Zhang, P. W. Stackhouse, S. K. Gupta, S. J. Cox, and J. C. Mikovitz. The validation of the gewex srb surface longwave flux data products using bsrn measurements. *Journal of Quantitative Spectroscopy and Radiative Transfer*, 150:134 – 147, 2015. ISSN 0022-4073. doi: http://dx.doi.org/10.1016/j.jqsrt.2014.07.013. URL http://www.sciencedirect.com/science/article/pii/S0022407314003185. Topical issue on optical particle characterization and remote sensing of the atmosphere: Part I.

Y. Zhang, W. B. Rossow, A. A. Lacis, V. Oinas, and M. I. Mishchenko. Calculation of radiative fluxes from the surface to top of atmosphere based on isccp and other global data sets: Refinements of the radiative transfer model and the input data. *Journal of Geophysical Research: Atmospheres*, 109(D19):n/a–n/a, 2004. ISSN 2156-2202. doi: 10.1029/2003JD004457. URL http://dx.doi.org/10.1029/2003JD004457. D19105.